Current status and perspectives of zinc-based absorbable alloys for biomedical applications

David Hernández-Escobar¹, Sébastien Champagne², Hakan Yilmazer³, Burak Dikici⁴ Carl J. Boehlert¹ Hendra Hermawan²,

- 1: Department of Chemical Engineering and Materials Science, Michigan State University, East Lansing, 48824, USA
- 2: Department of Mining, Metallurgical and Materials Engineering, Laval University, Quebec City, G1V 0A6, Canada
- 3: Department of Metallurgical and Materials Engineering, Yildiz Technical University, Istanbul, 34220, Turkey
- 4: Department of Metallurgical and Materials Engineering, Atatürk University, Erzurum, 25240, Turkey

Abstract

Absorbable metals have the potential to serve as the next generation of medical implant devices by safely dissolving in the human body upon tissue healing and bone regeneration. Their implementation in the market could greatly reduce the need of costly and risky additional surgeries for either implant replacement or removal, often required in current permanent implants containing titanium and stainless steel. Despite the extensive research done over the last two decades on magnesium (Mg) and iron (Fe) based alloys, they have not generally shown a satisfactory combination of mechanical properties, biocompatibility and controlled degradation rate in the physiological environment. Consequently, zinc (Zn) based alloys were introduced in the last few years as alternative materials to overcome the limitations of Fe and Mg-based alloys. The blend of different alloying elements and processing conditions have led to a wide variety of Zn-based alloys having tunable mechanical properties and corrosion rates. This review provides the most recent progress in the development of absorbable Zn-based alloys for biomedical implant applications. Their toxicological and metallurgical aspects, as well as their mechanical behavior and corrosion properties are presented and discussed, including their opportunities, limitations and future research directions.

Keywords: Absorbable, biodegradable, corrosion, implant, mechanical, metals, toxicology, zinc

Table of contents

1.	Introduction
2.	Toxicological aspects of zinc
3.	Metallurgy of zinc and its alloys
3.1	Conventional Zn alloys
3.2	Zn alloyed with nutrient elements
3.3	Zn alloyed with essential elements
3.4	Zn alloyed with other elements
4.	Mechanical properties of zinc and its alloys
5.	Corrosion behavior and properties of zinc and its alloys
6.	Pertinence of Zn-based absorbable alloys for biomedical applications 24
7.	Summary and concluding remarks25
8.	Acknowledgments
9.	References

1. Introduction

After decades of developing strategies to fight against corrosion of metallic biomaterials, there is currently an increasing interest to make use of corrodible metals in medical device applications. They are called biodegradable metals or absorbable metals ¹, metals that are expected to corrode gradually in-vivo by generating an appropriate host response, and then dissolve completely upon assisting tissue healing ². A gradual transfer of load to the healing tissue, and non-necessity of a second removal surgery are the two primary reasons why this category of metals are favorable alternatives to the existing corrosion resistant metal implants used for temporary interventions ³. To be considered as absorbable, a metal is required to corrode in a physiological environment and its corrosion products need to be non-toxic. Thereafter, it must have an optimum trade-off between maintaining strength and corroding within a required time frame. Iron (Fe), magnesium (Mg) and their alloys have been extensively studied as absorbable metals, mostly for cardiovascular and orthopaedic applications. Fe was used for making coronary stents and showed its safety and efficacy when tested in animals ⁴. Stents made of Mg alloys were clinically tested for critical limb ischemia in humans with some encouraging results 5, while some Mg bone screws are currently being examined through clinical trials in humans ⁶. Despite that, neither Fe nor Mg alloys have been able to successfully satisfy all the requirements demanded for absorbable implant applications.

Although the mechanical properties of Mg alloys can be improved significantly, they tend to corrode too rapidly in physiological environments, compromising the structural integrity of the implant device during the healing period ⁷. On the other hand, Fe alloys generally exhibit mechanical properties significantly greater than Mg alloys. However, they are characterized by slower corrosion rates, which unnecessarily prolongs the exposure time of the organism to the implant after healing and recovery have taken place. Moreover, the corrosion products of Fe tend to be stable in physiological environment, resulting in long-term retention ⁸. Consequently, zinc (Zn) has recently been introduced as an alternative to Fe and Mg, mainly due to its moderate corrosion rate in simulated body fluid ⁹. An in-vivo feasibility study highlighted the outstanding biocompatibility of Zn implants in vascular environments ¹⁰. Published works on Zn as an absorbable metal are on the rise with one of the latest reports being a one-year corrosion study of a pure Zn stent in a rabbit abdominal aorta model ¹¹. Many interesting findings have been reported, but more questions need answers, including: "Are we considering Zn as an escape from the

frustration with Mg and Fe?" This article provides a comprehensive review of the toxicological and metallurgical aspects, as well as, the mechanical and corrosion properties of Zn and Zn-based alloys to determine their pertinence to absorbable metals for biomedical applications.

2. Toxicological aspects of zinc

The role of Zn as an essential trace element in several physiological activities determines its importance for human health. In particular, Zn plays a fundamental role in multiple biochemical functions of the human body, including cell division, cell growth, wound healing, and the breakdown of carbohydrates ¹². Zinc deficiency has been linked to the impairment of physical growth and development in infants and young adults, to greater risk of infection, to impaired cognitive function, behavioral problems, and to impaired memory as well as learning disability ^{13,14}. However, an excess of Zn, (i.e. above its medium level of daily allowance of 15 mg for adult), may cause neurotoxicity problems ¹⁵.

Zinc is found in animal proteins, nuts, whole grains, legumes and yeast ¹⁶. It is released from food as free ions during digestion and absorbed in the small intestine by a carrier-mediated mechanism ¹⁷. Zinc is mainly present in the body as Zn²⁺, and its optimal concentration in human eukaryotic cells is around 10 ng/L. Apoptosis can be triggered when Zn levels fall below 0.06 ng/L, whereas toxic effects can be induced when Zn concentration rises above 60 ng/L ¹⁸. The absorbed Zn is carried by the portal system directly to the liver, and then released into systemic circulation for delivery to other tissues ¹⁹. About 60 % of Zn is stored in skeletal muscle, ~30 % in bones, and ~5 % is stored in the liver and skin, while the remaining percentage is distributed to other vital organs such as the brain, kidney, and pancreas ²⁰. Table 1 presents a series of symptoms/consequences of an inadequate Zn concentration in several different human organs and systems.

Table 1: Effects associated to Zn deficiency and excess in human organs and systems.

Organ / System	Zn deficiency	Zn excess	Ref.
Brain	Mental lethargy, neurosensory pathology, neuropsychiatric disorders, decreased nerve conduction	Neuronal death, lethargy, focal neuronal deficit	18,21,22
Heart	Congestive heart failure, ischemia/myocardial infarction,	Atrial premature beats, hypertension, hypovolemic shock	18,23

	arrhythmia, diabetic cardiomyopathy, atherosclerosis		
Liver	Alcoholic liver disease, viral liver disease	Chronic cholestatic liver disease, biliary cirrhosis	18,24
Kidney	Chronic kidney disease	-	25
Prostate	-	Higher risk of prostate adenocarcinoma	21,22
Gastrointestinal tract	-	Diarrhea, nausea, dysphagia, pharyngitis, esophagitis, epigastric pain	18,21,23
Epidermal system	Acrodermatitis enteropathica, alopecia, skin ulcers, delayed wound healing	-	21,26,27
Respiratory system	-	Metal fume fever, stridor, dysphonia, respiratory distress syndrome	18,21
Immune system	Impaired immune function, thymic atrophy, lymphopenia, increased susceptibility to infections	Altered lymphocyte proliferative response, reduction of chemotaxis and phagocytosis, immunosuppression	15,18,21,28
Reproductive system	Infertility, hypogonadism, testicular atrophy	-	21,23,24,26
Skeletal system	Growth retardation, abnormal calcification and development of fetal cranial bones	-	21,29

Healthy individuals are at higher risk of suffering from Zn deficiency than from Zn intoxication. Zinc deficiency can be inherited or acquired, and has been mainly related to insufficient dietary intake, but also to genetic disorders associated to malabsorption, such as acrodermatitis enteropathica, and chronic illnesses like sickle cell disease or anemia ²¹. Despite the list of adverse effects provided in Table 1, Zn is relatively harmless as compared to other metal ions. Only high Zn overdoses, i.e. ten times greater than the recommended daily dose ²³, typically lead to acute intoxication. In fact, many of the toxic effects reported from Zn are a consequence of copper (Cu) deficiency. This is often referred to as Zn-induced Cu deficiency, which is caused by a competitive absorption of Zn and Cu within enterocytes, and results in reduced Cu absorption when there is an excess of Zn ^{18,21}.

Most of the Zn in circulation is bound to albumin forming the serum Zn that represents only 0.1 % of the amount of Zn present in the body ¹⁴. Zinc homeostasis, or maintaining a constant state of cellular Zn, is essential for human survival. It is achieved by the synergetic adjustments in gastrointestinal Zn absorption (20-40 %), urinary (0.5 mg/day) and intestinal (1-3 mg/day) excretion, sloughing mucosal cells and integument ^{16,30}. Typically, human Zn intakes range from 107 to 231 μmol/day (~14-30 mg/kg), but Zn homeostasis can be achieved with as little as 2.8 mg/kg or as much as 40 mg/kg ³¹. Nutritional supplements were developed to overcome the undesirable consequences of Zn deficiency. The average adult human contains 2-3 g of Zn, of which about 0.1% is replenished daily ³². This leads to an average recommended dietary intake ranging between 5-20 mg/day, depending on gender and age. Growing children and pregnant women generally require higher amounts than mature adults ¹⁸. Thus, the need of supplemental Zn, as well as the right dose amount, must be carefully evaluated in a case-by-case basis, as chronic Zn toxicity has been reported from excessive consumption of Zn supplements ³².

Furthermore, the presence of absorbable implants that corrode over time also must be accounted for when considering Zn supplementation, as they would act as an extra source of Zn into the bloodstream, which may induce systemic toxicity. The cytocompatibility of absorbable Zn and its alloys has been studied in view of its applications for bone and vascular implants. Murni, et al. ³³ carried out a thorough in-vitro cytotoxicity evaluation of absorbable Zn-3Mg (wt.%) toward normal human osteoblast cells in view of future applications for bone implants. At a concentration of 0.75 mg/ml (0.49 ppm Zn and 10.75 ppm Mg), the Zn-3Mg (wt.%) alloy extract exhibited adjustable cytotoxic effects on normal human osteoblast cells. In a comparative study of Zn exposure to three vascular cell types, Shearier et al. 34 determined the LD50 values of 50 µM for human dermal fibroblast, 70 µM for human aortic smooth muscle cells, and 265 µM for human endothelial cells, and demonstrated a Zn dose-dependent effect on cell spreading and migration, suggesting that both adhesion and cell mobility may be hindered by free Zn²⁺. Ma, et al. ³⁵ showed an interesting biphasic effect of Zn²⁺ on human smooth muscle cells up to 24 h. At lower concentrations (<80 µM), Zn²⁺ had no adverse effects on cell viability, but cells treated with higher Zn²⁺ concentrations (80-120 μM) had opposite cellular responses and behaviors which affected functional genes. Although the in-vitro studies indicated a lack of understanding of how Zn and Zn²⁺ affect surrounding cells, the in-vivo studies indicated the outstanding biocompatibility of Znbased implants in vascular environments.

Xiao, et al. ³⁶ conducted in-vitro and in-vivo experiments of pure Zn and Zn-0.05Mg (wt.%), showing a homogenous in-vitro degradation rate and no inflammatory response in the in-vivo rabbit model. Moreover, new bone tissue was formed at the bone/implant interface, and strong antibacterial activity was found against Escherichia coli and Staphylococcus aureus. Alternatively, Bowen, et al. ¹⁰ examined the in-vivo degradability of pure Zn wire in the abdominal aorta of rats and showed that the wire remained intact for four months before the corrosion accelerated. The corrosion was largely compact and comprised Zn oxide interspersed in Zn carbonate (Figure 1a). They further demonstrated that metallic Zn did not provoke any response associated to restenosis as the progression in neointimal tissue thickness over 6.5 months and the presence of smooth muscle cells near the Zn implant were suppressed by Zn corrosion products and led to a benign neointimal formation and a healthy artery (Figure 1b) 37. For long-term implantation, the inflammatory profile of Zn wires was dictated by the corrosion characteristics where alloying with aluminum (Al) increased the activity of macrophages that penetrated and remained viable within the corrosion layer (Figure 1c) ³⁸. Yang, et al. ¹¹ conducted a one-year implantation study of a pure Zn stent in a rabbit abdominal agrta model and found that the intrinsic properties of Zn enabled a match between its corrosion and artery healing process, while maintaining the stent's mechanical integrity for six months (Figure 1d). All these studies highlight a favorable physiological behavior, and thus, it is concluded that Zn has a promising potential to be used for absorbable stents.

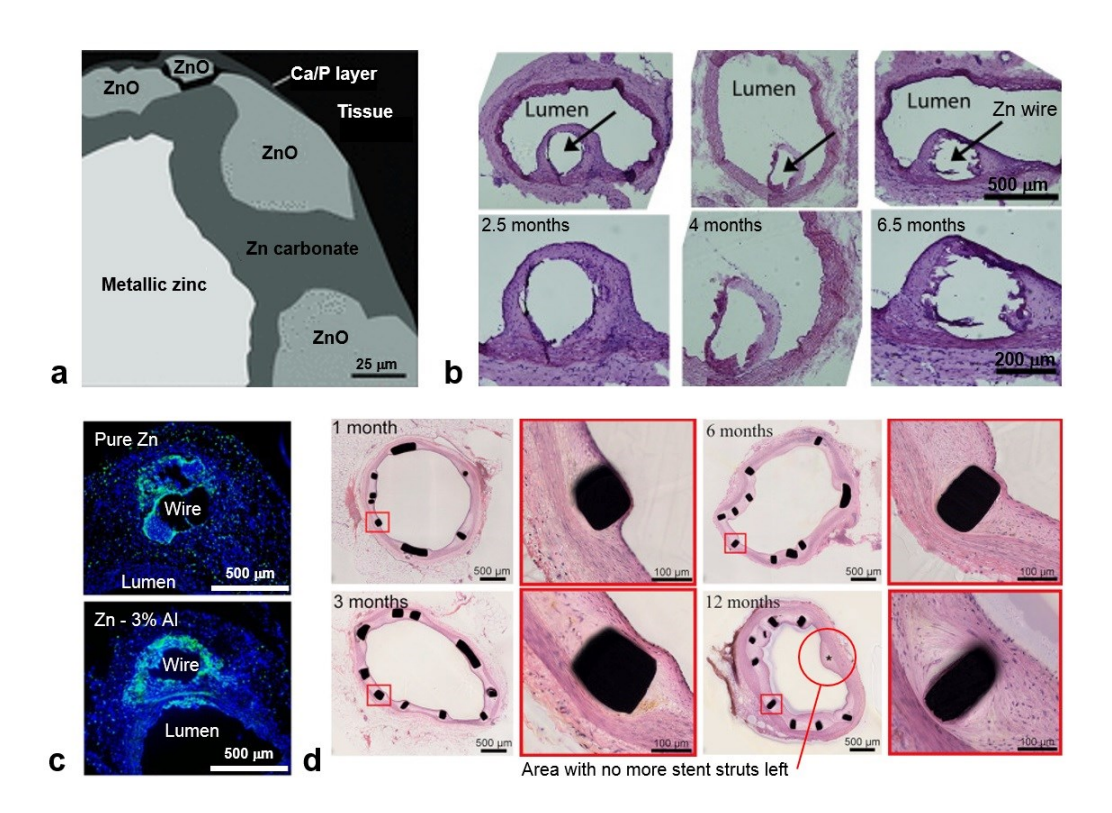


Figure 1: Selected in-vivo results of Zn implants reported in the literature: (a) backscattered electron image of cross-sectional Zn wire after implantation in abdominal aorta of rat for 4.5 months, (b) histological sections from excised Zn wires after residence in the arterial lumen for 2.5, 4 and 6.5 months, (c) CD68 (green) and CD11/b (red) labeling of cross-sections containing the explanted artery and the pure Zn and Zn-3Al wires at 6 months, (d) histological sections of abdominal aorta after 1, 3, 6, and 12 months implantation of Zn stents. Adapted from 10,11,37,39.

3. Metallurgy of zinc and its alloys

Zinc has an atomic number of 30, a molar mass of 65.38 g/mol, a density of 7.13 g/cm³, a melting temperature of 419.5 °C, and exhibits a single oxidation state (+2) ⁴⁰. Zinc is the fourth most widely used metal after Fe, Al and Cu, and nearly 14 million metric tons of Zn were produced annually in 2016 ⁴¹. Zinc and its alloys are used as structural components for engineering applications in a wide variety of formats. Nearly half of the total world consumption of Zn is in the form of coatings for the corrosion protection of steel components. This is performed by hot-dip galvanizing in a 450 °C bath of molten Zn or by electroplating in a cold electrolytic bath, where the life of the protective Zn coatings is proportional to its thickness ⁴². The second-leading use of Zn is in brass and cast alloys, which represent about 30% of the market, and the remaining use is in wrought alloys and in the production of Zn oxide for rubber manufacturing, pharmaceuticals and batteries ⁴³.

3.1 Conventional Zn alloys

Brass is an alloy made up of Zn and Cu which can be classified into: α (< 35 wt. %Zn), α - β (35-45 wt. % Zn), and $\beta'(>45$ wt. % Zn) brasses. α brasses are ductile and easily cold worked, while those with higher Zn contents are harder and can only be hot worked or cast and thus have limited industrial application ⁴⁴. Lead is usually added to enhance workability, and arsenic may be added to make brass more stable in certain environments 44. In the cast Zn alloys, there are two main families based on Zn-Al system: ZA (Zn-Al) and Zamak (Zn-Al-Mg-Cu) alloys. Addition of Al to Zn reduces the grain size and increases the strength. In general, Zn-Al alloys are relatively easy to die cast at low temperatures and allow further machining at a low cost. They have good resistance to surface corrosion and exhibit greater strengths than many other die-cast alloys ^{45,46}. As-cast Zn alloys are in a metastable condition after manufacturing due to a very rapid cooling. This produces natural aging, resulting in a slight increase of elongation-to-failure (ε_f) and decrease of strength over a period of about 10 years at room temperature (RT). Aging treatments are also used to accelerate the transition to the equilibrium microstructure after casting 45. The remaining class of wrought Zn alloys are mostly supplied as rolled sheet products. Copper and titanium are usually added to improve the creep resistance at RT. Rolled Zn can be easily joined by soldering and resistance welding and it is widely used in coinage and dry battery cells. Other manufacturing processes, such as forging and extrusion, can be also applied, although they have found limited application ⁴⁷.

Despite the wide selection of Zn alloys having good mechanical and corrosion properties, those intended for biomedical applications must be designed with non-toxic alloying elements. Consequently, the ZA and Zamak alloy series cannot be considered as they contain large amounts of Al that has been reported to be harmful to bone, neurons and osteoblasts ⁴⁸, and also associated with dementia and Alzheimer disease ^{49,50}. More acceptable alloying elements include the nutrient elements present in the bone matrix (e.g. Mg, Ca and Sr) and the essential elements in human physiological activities (e.g. Cu and Mn), which have been used for developing Zn-based absorbable alloys. Limited amounts of Al is still considered for small implants where long term corrosion may not cause toxic effects ^{51,52}. The following sections describe the metallurgy of Zn-based absorbable alloys for biomedical applications.

3.2 Zn alloyed with nutrient elements

Included in this class are Zn-Mg, Zn-Ca, Zn-Sr alloys. According to the Zn-Mg phase diagram (Figure 2a), the maximum solubility of Mg in Zn is about 0.1 wt.% at 364 °C and it becomes negligible at RT. Consequently, minimal addition of Mg to Zn lead to the formation of Mg₂Zn₁₁ intermetallic compounds. Zn-Mg binary alloys containing 0.15, 0.5, 1 and 3 wt.% Mg were studied by Mostaed el al. ⁵² where the alloys were cast at 500 °C, annealed at 350 °C for microstructure homogenization, water-quenched and hot extruded to obtain stent-sized mini tubes. In agreement with the Zn-Mg phase diagram, the microstructures of hypoeutectic Zn-0.15Mg, Zn-0.5Mg and Zn-1Mg consisted of Zn dendritic grains embedded in a eutectic matrix of Zn and Mg₂Zn₁₁. In contrast, Zn-3Mg exhibited a fully eutectic microstructure with fine alternate lamellae of Zn and Mg₂Zn₁₁. In all the alloys, increasing the Mg content was found to decrease the grain size ⁵². Jin et al. ⁵³ reached the same conclusion from extruded and drawn Zn-Mg alloys containing 0.08, 0.005 and 0.002 wt.% Mg.

The addition of Ca and Sr to hypoeutectic Zn-Mg alloys was investigated independently by Liu et al. ⁵⁴ for Zn-1.5Mg-0.1Ca/Sr (wt.%) and Li et al. ⁵⁵ for Zn-1Mg-1Ca/Sr (wt.%) ternary alloys, to study the effect of hot extrusion and hot rolling. Precipitated phases of Mg₂Zn₁₁, CaZn₁₃ and SrZn₁₃ were identified in Zn-Mg-Ca/Sr ternary alloys, which lead to finer and more homogenous microstructures. The effect of Mn was investigated by Liu et al. ⁵⁶ as a candidate for novel ternary Zn-Mg-Mn absorbable alloys. The microstructures of the alloys contained eutectic mixtures of Zn, MgZn₂ and Mn. In all cases, the addition of Ca, Sr and Mn improved the tensile strength of the Zn-Mg based alloys.

In the Zn-Ca system (Figure 2b) there is no solubility of Ca in Zn; small addition of Ca to Zn results in the formation of CaZn₁₃ intermetallic phase. This system has only been studied by Li et al. ⁵⁷ where the as-cast microstructure of Zn-1Ca (wt.%) was composed of hexagonal close-packed Zn dendrites and a eutectic mixture of Zn and CaZn₁₃. The alloy showed an improved tensile strength as compared to pure Zn. Further addition of Sr and subsequent hot-extrusion and hot-rolling processes produced a more homogenous and fine-grained microstructure as compared to the as-cast counterpart ⁵⁵. Like Ca, Sr has no solubility in Zn (Figure 2c), such that small additions of Sr to Zn lead to the formation of the intermetallic compound SrZn₁₃. Li et al. ⁵⁷ observed primary Zn dendrites and a eutectic mixture of Zn and SrZn₁₃ in the as-cast microstructure of Zn-1Sr (wt.%)

alloy. Further hot-extrusion and hot-rolling effectively increased the alloy's strength and ε_f as compared to the as-cast condition.

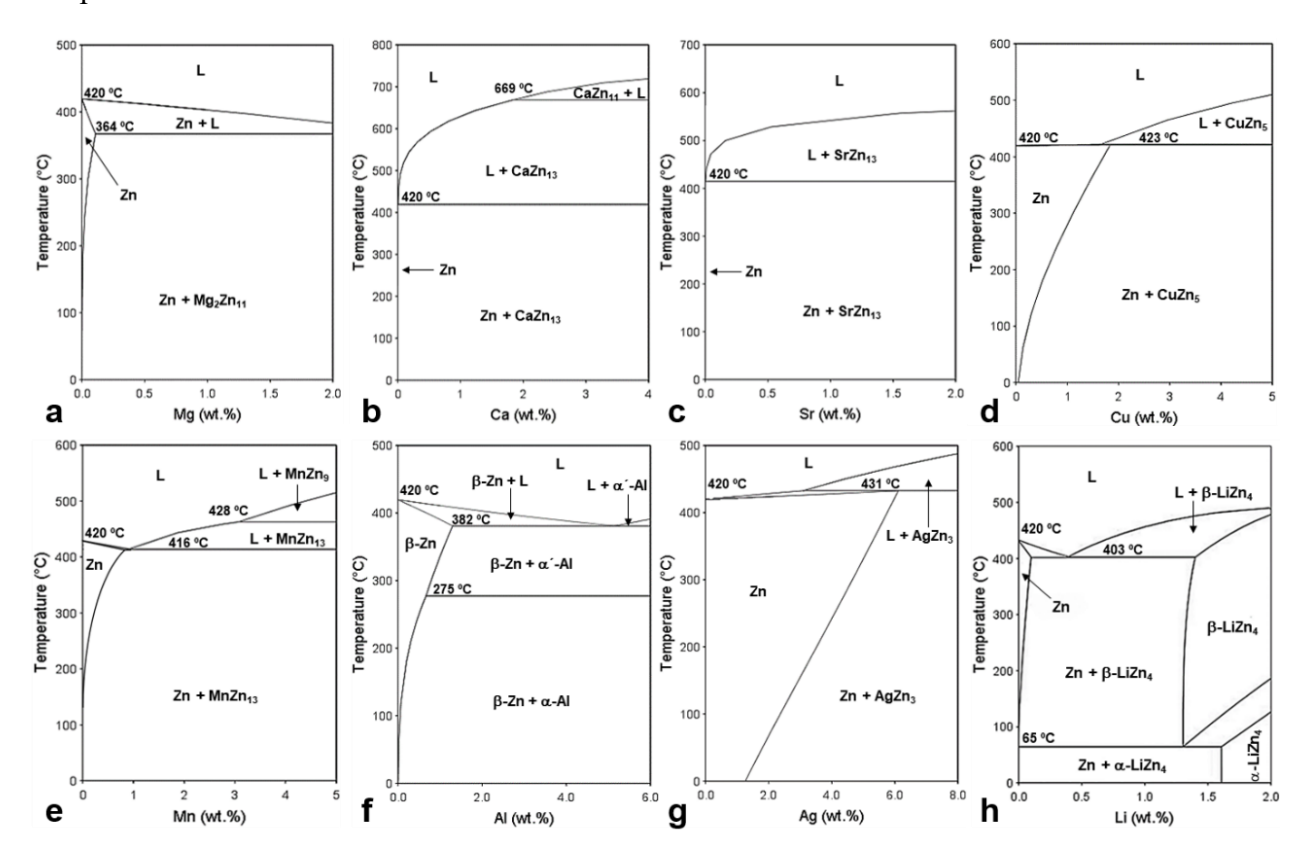


Figure 2: Equilibrium phase diagrams showing regions of interest for the development of Zn-based absorbable alloys: a) Zn-Mg, b) Zn-Ca, c) Zn-Sr, d) Zn-Cu, e) Zn-Mn, f) Zn-Al, g) Zn-Ag, h) Zn-Li. Adapted from ⁵⁸.

3.3 Zn alloyed with essential elements

Cu has a maximum solubility of about 2 wt. % in Zn at 423 °C (Figure 2d) where at that temperature the eutectic reaction forms a mixture of Zn and CuZn₅ phases. Zn-xCu (x = 1, 2, 3, 4 wt. %) binary alloys were investigated by Tang et al. ⁵⁹ and Niu et al. ⁶⁰ for absorbable cardiovascular implants. The as-cast microstructures consisted of dendritic CuZn₅ phase embedded in primary Zn matrix, with increasing dendritic volume fraction at higher Cu concentrations. Homogenization of the alloys at 360°C did not alter the microstructure, which revealed the thermal stability of the CuZn₅ intermetallic. Further hot-extrusion processing caused grain refinement, especially in the regions closer to the CuZn₅ phase, due to dynamic recrystallization. The effect of small Mg additions to the Zn-Cu system was investigated through a series of Zn-3Cu-xMg (x = 0, 0.1, 0.5, 1.0 wt. %) ternary alloys by Tang et al. ⁶¹. Increasing Mg concentration gradually refined the grain size and

led to a more homogenous microstructure, resulting in higher tensile strength and a more uniform corrosion. Yue et al. 62 studied the effect of Fe in the Zn-Cu system in Zn-3Cu-xFe (x = 0.5, 1.0 wt.%) ternary alloys, and found that the addition of Fe gave rise to the formation of coarse FeZn₁₃ and CuZn₅ particles, which caused distortion of the microstructure uniformity accompanied by a deterioration of both tensile strength and $\epsilon_{\rm f}$.

Mn has a maximum solubility in Zn of about 0.8 wt. % at 416 °C (Figure 2e). A solid solution of Zn and MnZn₁₃ intermetallic form at that temperature due to a eutectic reaction. Zn-xMn binary alloys (x = 0.2, 0.4, 0.6 wt.%) were studied by Sun et al. 63 . The Zn-0.2Mn alloy showed only Zn rich phases, whereas the MnZn₁₃ intermetallic was identified in the Zn-0.4Mn and Zn-0.6Mn alloys. The average grain size of the hot-extruded alloys decreased notably with the addition of 0.2 wt.% Mn and remained practically constant with higher Mn content. Twinning volume fraction gradually decreased with increasing Mn content, while a dominant basal texture was maintained, independently of Mn content. Consequently, dislocation movement was enhanced with higher Mn content resulting in an increase of the ε_f at the expense of tensile strength. Sotoudeh Bagha et al. 64 prepared Zn-xMn (x = 4, 24 wt.%) alloys via powder metallurgy and found a microstructure consisting of nano-sized crystallites with MnZn₁₃ and MnZn₃ second phases, which contributed to an increased compression strength.

3.4 Zn alloyed with other elements

Al has a maximum solubility in Zn at about 1 wt. % at 382 °C (Figure 2f). A eutectic reaction forms a mixture of β -Zn and α '-Al. The latter is not stable below 275 °C and transforms into α -Al through a monotectoid reaction. Zn-xAl (x = 0.5, 1 wt. %) binary alloys were explored by Mostaed et al. ⁵² for absorbable stent applications. The as-cast microstructures consisted of a Zn matrix with a small content of a Zn-Al eutectoid mixture, located mainly at the grain boundaries, which act as pinning points and therefore delay grain growth leading to finer grain sizes. Further solution treatment at 350°C was found to dissolve the eutectic constituent in the Zn-rich matrix, forming a supersaturated solid solution. Despite the toxicity concern of Al, higher Al-containing alloys, i.e. Zn-xAl (x = 1, 3, 5 wt.%) were investigated by Bowen et al. ⁵¹ also for stent applications under a consideration that the presence of Al in such a tiny device with a long corrosion time may not be toxic. Bakhsheshi-Rad et al. ⁶⁵ added Mg into the system to form Zn-0.5Al-xMg (x = 0.1, 0.3 and 0.5 wt.%) ternary alloys. Its microstructure consisted of fine lamellar of α -Zn and Mg₂(Zn, Al)₁₁.

Further addition of Bi in Zn-0.5Al-0.5Mg-xBi (x = 0.1, 0.3 wt.%) alloys formed Mg₃Bi₂ phase that increase strength in expense of corrosion resistance ⁶⁶.

Zinc has also been alloyed with Ag knowing that Ag is soluble in Zn at about 6 wt. % at 431 °C, where a peritectic reaction transforms AgZn₃ and liquid into a Zn solid solution (Figure 2g). Sikora-Jasinska et al. ⁶⁷ observed that the as-cast microstructure of Zn-xAg (x = 2.5, 5, 7 wt.%) alloys consisted of a primary Zn matrix and AgZn₃ dendrites, with an increasing volume fraction of the latter at higher Ag contents. After solution treatment at 410 °C, the AgZn₃ dendrites were fragmented into equiaxed particles uniformly dispersed through the Zn matrix. Upon 6h and 12h solution treatments for the 2.5-5 and 7 wt.% Ag alloys, respectively, the AgZn₃ phase was dissolved forming a supersaturated solid solution of Ag in Zn. Further hot-extrusion significantly reduced the grain size of the alloys, and it was found that Ag contents above 5 wt. % were needed for complete recrystallization to achieve a uniformly refined microstructure.

Lithium is another element added to Zn, and its maximum solubility in Zn is only about 0.1 wt. % at 403 °C (Figure 2h). At that temperature, a eutectic reaction transforms the liquid phase into Zn and β-LiZn₄, which further transforms to α-LiZn₄ below 65 °C. Zhao et al. ⁶⁸ studied Zn-xLi (x = 0.2, 0.4, 0.7 wt.%) binary alloys, which correspond to hypoeutectic, eutectic and hypereutectic compositions, respectively. The as-cast microstructure of the Zn-0.2Li exhibited Zn+LiZn₄ dispersed in the Zn matrix, whereas for lower Li addition, lamellar Zn+LiZn₄ eutectic microconstituents decorated the Zn grain boundaries. After hot rolling, the Zn-0.4Li and Zn-0.7Li alloys exhibited a severe rolling texture with finer dendrites and grains, while Zn-0.2Li presented equiaxed grains due to dynamic recrystallization.

4. Mechanical properties of zinc and its alloys

Mechanical properties of Zn, conventional Zn alloys and Zn-based absorbable alloys after different thermomechanical treatments are presented in Table 2. In general, conventional die-cast Zn alloys (ZA and Zamak) possess mechanical properties comparable to, and in some cases exceeding, those of commonly used Fe, Al and Cu casting alloys. However, they cannot be considered for biomedical applications. The inherently poor mechanical properties of pure Zn, i.e. tensile strength < 20MPa, elongation < 0.5% 55, can be improved by alloying and further thermomechanical or severe plastic deformation (SPD) processing. It can be observed that a small addition of 0.5 wt.% Mg significantly increases the tensile strength and ε_f from 18 MPa and 0.3% to 297 MPa and 13%,

respectively [53], [60]. An increasing Mg content up to 3 wt.% gradually improves the strength and hardness, although this comes with a decrease in elongation due to the larger volume fraction of the Mg_2Zn_{11} phase. Nevertheless, increasing the amount of alloying element does not always improve mechanical properties, as is the case of Zn-Mn alloys. Even though the volume fraction of the $MnZn_{13}$ intermetallic compound increased with Mn content, and it is generally associated to higher strength, Zn-0.6Mn (wt.%) exhibited gradually lower tensile strength and higher ϵ_f than Zn-0.4Mn (wt.%) and Zn-0.2Mn (wt.%) respectively, associated to a significant reduction in the twinning volume fraction with decreasing Mn content.

Table 2: Mechanical properties of Zn, conventional Zn alloys and Zn-based absorbable alloys.

Alloy (wt.%)	Yield strength (MPa)	Tensile strength (MPa)	Elongation-to- failure (%)	Hardness Vickers (HV)	Ref.
Zn	10 ± 2	18 ± 3	0.3 ± 0.1	38 ± 1	55
Zn *, a	33 ± 7	64 ± 15	3.6 ± 1.8	-	55
$Zn^{**, a}$	30 ± 7	50 ± 9	5.8 ± 0.8	39 ± 4	55
Zn *	51 ± 4	111 ± 5	60 ± 6	34 ± 2	52
		Conventional Zn a	lloys		
Zamak 3	221	283	10	93 b	69
Zamak 7	221	283	13	86 ^b	69
Zamak 5	228	328	7	102 b	69
Zamak 2	-	359	7	112 ^b	69
ZA-8 ⁺	290	374	8 ± 2	116 ^b	69
ZA-12 ⁺	320	404	5 ± 2	112 ^b	69
ZA-27 ⁺	376	425	2 ± 1	135 b	69
		Zn-based absorbable	alloys		
Zn-0.05Mg *	160	225	26	-	36
Zn-0.15Mg *	114 ± 8	250 ± 9	22 ± 4	52 ± 5	52
Zn-0.5Mg *	159 ± 9	297 ± 7	13 ± 1	65 ± 4	52
Zn-1Mg *	180 ± 7	340 ± 16	6 ± 1	75 ± 4	52
Zn-1Mg HE	316	435	35	-	70
Zn-1.2Mg	117 ± 1	130 ± 6	1.4 ± 0.6	93 ± 7	71
Zn-1.2Mg *	220 ± 15	363 ± 5	21.3 ± 2.3	96 ± 7	71
Zn-1.5Mg	112 ± 3	151 ± 14	1.3 ± 0.2	150 ± 30	54
Zn-3Mg	65 ± 9	84 ± 9	1.3 ± 0.3	200 ± 7	72
Zn-3Mg ECAP	220 ± 3	205 ± 4	6 ± 1	186 ± 4	72

Zn-1Mg-1Ca ^a	80 ± 9	131 ± 16	1 ± 0.3	92 ± 10	55
Zn-1Mg-1Ca *, a	205 ± 10	257 ± 13	5.2 ± 1	-	55
Zn-1Mg-1Ca **, a	138 ± 9	198 ± 20	8.5 ± 1.3	107 ± 10	55
Zn-1.5Mg-0.1Ca	174 ± 15	241	1.7	150 ± 30	54
Zn-1Mg-0.1Sr	109 ± 14	132 ± 10	1.4 ± 0.4	94 ± 7	73
Zn-1Mg-0.1Sr **	197 ± 13	300 ± 6	22.5 ± 2.5	104 ± 10	73
Zn-1Mg-1Sr ^a	87 ± 7	138 ± 9	1.3 ± 0.2	85 ± 2	55
Zn-1Mg-1Sr *, a	202 ± 5	253 ± 18	7.4 ± 1.3	-	55
Zn-1Mg-1Sr **, a	140 ± 10	201 ± 10	9.7 ± 1	92 ± 5	55
Zn-1.5Mg-0.1Sr	130 ± 8	209 ± 10	2.0 ± 0.2	150 ± 20	54
Zn-1Mg-0.1Mn	114	132	1.1	98	56
Zn-1Mg-0.1Mn **	195	299	26.1	108	56
Zn-1Ca	119 ± 7	165 ± 14	2.1 ± 0.2	73 ± 7	57
Zn-1Ca-1Sr ^a	86 ± 5	140 ± 9	1.2 ± 0.2	91 ± 12	55
Zn-1Ca-1Sr *, a	212 ± 15	260 ± 15	6.7 ± 1.1	-	55
Zn-1Ca-1Sr **, a	144 ± 9	203 ± 10	8.8 ± 1.2	87 ± 7	55
Zn-1Sr	120 ± 6	171 ± 14	2.0 ± 0.2	62 ± 7	57
Zn-1Sr *, c	217 ± 9	264 ± 10	10.6 ± 1.1	-	57
Zn-1Sr **, c	190 ± 5	230 ± 10	19.7 ± 1.7	62 ± 5	57
Zn-1Cu *	149 ± 1	186 ± 1	21.0 ± 4.4	-	59
Zn-2Cu *	200 ± 4	240 ± 1	46.8 ± 1.4	-	59
Zn-3Cu *, e	247 ± 8	288 ± 4	50.6 ± 2.8	67 ± 1	62
Zn-3Cu-0.1Mg *, d	340 ± 15	360 ± 15	5 ± 1	-	61
Zn-3Cu-0.5Mg *, d	400 ± 10	420 ± 5	2 ± 1	-	61
Zn-3Cu-1Mg *, d	425 ± 5	440 ± 5	1 ± 0.5	-	61
Zn-3Cu-0.5Fe *, e	232 ± 3	284 ± 2	32.7 ± 4.2	76 ± 1	62
Zn-3Cu-1Fe *, e	222 ± 6	272 ± 7	19.6 ± 1.4	82 ± 1	62
Zn-4Cu *	250 ± 10	270 ± 10	51 ± 2	-	60
Zn-0.5Al	-	79 ± 2	1.5 ± 0.1	71 ± 2	65
Zn-0.5Al *	119 ± 2	203 ± 10	33 ± 1.2	59 ± 6	52
Zn-1Al*	134 ± 6	223 ± 4	24 ± 4.2	73 ± 5	52
Zn-1Al **, f	190	220	24	-	51
Zn-3A1 **, f	200	240	31	-	51
Zn-5Al **, f	240	308	16	-	51
Zn-4Al-1Cu	210	171	1	80	9
Zn-0.5Al-0.1Mg	-	87 ± 3	1.6 ± 0.1	79 ± 3	65

Zn-0.5Al-0.3Mg	-	93 ± 3	1.7 ± 0.1	87 ± 3	65
Zn-0.5Al-0.5Mg	-	102 ± 4	2.1 ± 0.1	94 ± 4	65
Zn-0.2Mn *	132	220	48	-	63
Zn-0.4Mn *	123	198	54	-	63
Zn-0.6Mn *	118	182	71	-	63
Zn-2.5Ag *, g	147 ± 7	203 ± 5	35 ± 4	-	67
Zn-5Ag *, g	210 ± 10	252 ± 7	37 ± 3	-	67
$Zn-7Ag^{*,g}$	236 ± 12	287 ± 13	32 ± 2	-	67
Zn-0.2Li **, h	240 ± 10	360 ± 15	14.2 ± 2.0	98 ± 6	68
Zn-0.4Li **, h	425 ± 15	440 ± 5	13.8 ± 2.9	115 ± 7	68
Zn-0.7Li **, h	475 ± 50	565 ± 2	2.4 ± 0.4	137 ± 8	68

As cast; *As die-cast; *As hot-extruded; ** As hot-rolled; ** Hydrostatic extrusion; *ECAP Equal channel angular pressing; a Data from 55; b Estimated from Hardness Brinell HB 10/500 in 74; c Data from 57; d Data from 61; e Data from 62; f Data from 51; g Data from 67; h Data from 68.

Overall, both hot-extrusion and hot-rolling were effective in increasing the yield strength, tensile strength and hardness of binary and ternary Zn-based alloys containing Mg, Ca, Sr, Cu, Al, Ag and Li. For instance, the tensile strength and ε_f of as-cast Zn-1Sr were simultaneously enhanced from 171 MPa and 2% to 264 MPa and 10.6% by hot-extrusion, and to 230 MPa and 19.7% by hot-rolling ⁵⁷. Similarly, the application of SPD techniques, such as hydrostatic extrusion (HE) and equal-channel angular pressing (ECAP), have shown potential for achieving nanograin-sized microstructures that lead to a concurrent increase of the tensile strength and ε_f in Zn-Mg alloys ^{70,72}. In fact, the exceptional grain refinement obtained in SPD-processed materials is generally assumed to enhance not only the mechanical behavior, but also the corrosion resistance ⁷⁵. Therefore, with the adequate combination of alloying elements and further thermomechanical processing, it is feasible that the structural requirements of absorbable Zn alloys for future medical applications will be satisfied.

Nonetheless, it should be noted that implantable medical devices, i.e. stents, wires, plates and screws, may differ significantly in terms of their morphology and mechanical constraints. Thus, it is expected that manufacturing absorbable metal implants with a similar composition for different applications, may require the processing parameters to be tailored accordingly. The grain size and shape, the secondary phases, and their distribution and crystal texture are the primary microstructural features that can be altered to reach the benchmark values required for absorbable applications. In addition, as the implantation time progresses, the absorbable metal is corroded,

and deterioration of the mechanical properties is expected. However, the structural integrity of the implant must be guaranteed during the healing period, and then, gradually transferred to the host tissue/bone as corrosion advances. To avoid catastrophic failure of the implant, it is vital to consider any additional loading condition on the implantation site, which could alter the time intervals required for the healing process due to stress-corrosion.

5. Corrosion behavior and properties of zinc and its alloys

Throughout history, Zn has been widely used as a disposable or sacrificial metal in the cathodic protection of metallic structures, particularly those made of steel. It is often used either as a sacrificial anode or as a protective coating on bridges and boats. Zinc has also been used as a self-healing roofing material for more than a century ⁷⁶. Therefore, the knowledge about the corrosion mechanisms of Zn in atmospheric and marine conditions is already well developed and well understood. In general, the corrosion that occurs under atmospheric conditions is the result of an aqueous environment. Among all the possible forms of corrosion, Zn is more prone to uniform, galvanic, pitting and intergranular corrosion. In the case of galvanic corrosion, more noble metals when alloyed with Zn, usually result in an increase in the corrosion rate ⁷⁷.

The corrosion evaluation of Zn-based absorbable alloys, as well as other materials targeted for biomedical applications, is done primarily in a controlled in-vitro setting before continuing to a more complex in-vivo implantation. The in-vitro corrosion testing is done using an electrolyte having a chemical composition that simulates human blood plasma as per the ASTM standard F2129 78 . The commonly used physiological electrolytes are Kokubo's solution, simulated body fluid (SBF), Ringer's solution, and Hanks' solution. Regardless of the electrolyte used, the corrosion mechanism of Zn is governed by the reactions in Equation 1 - 4 54 . Different from corrosion of Mg, no hydrogen gas evolution takes place during the corrosion of Zn. The high concentration of chloride ions in physiological electrolyte tends to break the equilibrium between the dissolution and formation of corrosion products, as per Equation 5 and 6 54 . The dissolution of $Zn(OH)_2$ and ZnO corrosion products into soluble chloride salts, leaves the fresh metal surface exposed directly to the electrolyte, which promotes its further dissolution. Carbonate and phosphate ions have also been found on the corrosion products of Zn and Zn-based alloys 79,80 .

Anodic reaction:
$$Zn \rightarrow Zn^{2+} + 2e^{-}$$
 (1)

Cathodic reaction:
$$O_2 + 2H_2O + 4e^- \rightarrow 40H^-$$
 (2)

$$Zn(OH)_2$$
 formation: $2Zn^{2+} + 4OH^- \rightarrow 2Zn(OH)_2$ (3)

ZnO formation:
$$Zn(OH)_2 \rightarrow ZnO + H_2O$$
 (4)

$$6Zn(OH)_2 + Zn^{2+} + 2Cl^- \rightarrow 6Zn(OH)_2 \cdot ZnCl_2$$
 (5)

$$4ZnO + 4H_2O + Zn^{2+} + 2Cl^{-} \rightarrow 4Zn(OH)_2 \cdot ZnCl_2$$
 (6)

Besides the chemical composition, the pH of the electrolyte plays an important role in the corrosion of Zn ⁸¹. According to the modified Pourbaix diagram presented by Thomas et al. ⁸² (Figure 3), both corrosion and pitting phenomena have been observed in Zn for pH values from 1 to 13. However, in the pH range of 7-10, the lower cathodic reaction rates reduce the overall corrosion rates such that the surface oxides thermodynamically predicted do not form an effective protection layer ⁸². This indicates that Zn metal immersed in a physiological electrolyte pH of ~7.4 will dissolve over time, as desired for an absorbable implant.

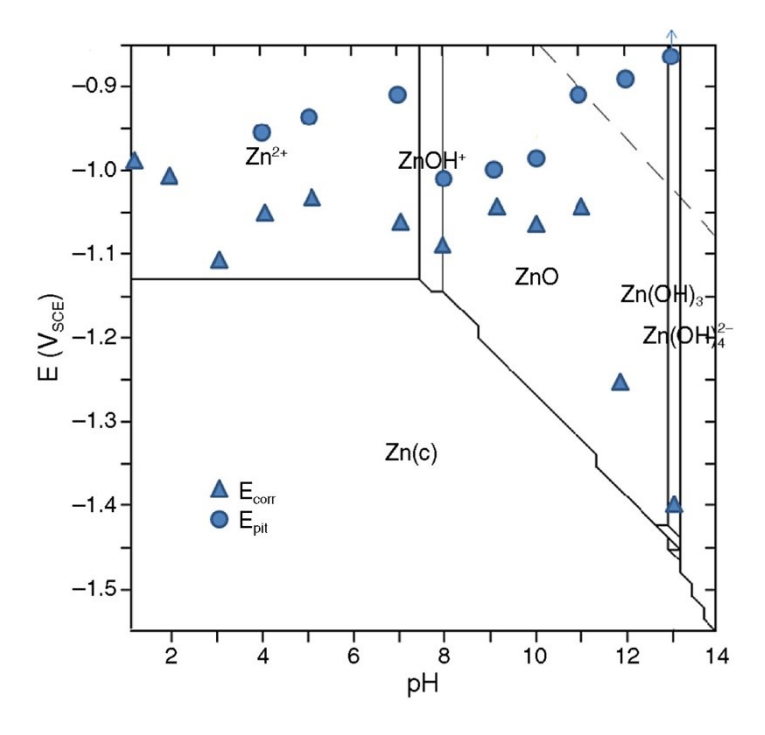


Figure 3: Modified potential-pH diagram of Zn in 0.1 M chloride environment. Adapted from 82.

Torne et al. ⁷⁹ were the first to study the electrochemical properties of pure Zn in whole blood and blood plasma, and compared their results to those in Ringer's and phosphate buffered saline (PBS) solution. The metal had a stabilized potential during the first hours of immersion in both PBS and

Ringer's solution, while never stabilized in plasma and blood. The corrosion rate increased with immersion time for the two simulated body fluids, whereas it decreased for the two real body fluids. Table 3 provides a comparative summary of electrochemical data obtained from in-vitro corrosion studies of Zn and Zn-based alloys, which have been documented in the literature.

Table 3: Corrosion rates of different Zn and Zn-based alloys from immersion (CRI) and electrochemical (CRE) experiments.

Alloy (wt.%)	CRI (mm/year)	E _{corr} (V)	I _{corr} (μΑ/cm²)	CRE (mm/year)	Electrolyte solution	Ref.
Zn *	0.15	-0.914±0.12	44.0±7.14	0.653		36
Zn-0.05Mg *	0.15	-0.938±0.08	49.1±2.28	0.728	SBF	36
Zn	-	-0.99	9.20	0.137 ± 0.004		52
Zn *	0.074 ± 0.004	-0.98	8.98	0.134 ± 0.008		52
Zn-0.15Mg	-	-1.03	11.52	0.172 ± 0.003		52
Zn-0.15Mg *	0.079 ± 0.004	-1.01	10.98	0.164 ± 0.003		52
Zn-0.5Mg	-	-1.05	11.73	0.175 ± 0.004	TT 1	52
Zn-0.5Mg *	0.081 ± 0.002	-1.02	11.01	0.164 ± 0.008	Hanks	52
Zn-1Mg	-	-1.07	11.88	0.177 ± 0.007		52
Zn-1Mg *	0.083 ± 0.004	-1.05	11.32	0.169 ± 0.006		52
Zn-3Mg	-	-0.98	9.01	0.135 ± 0.006		52
Zn-3Mg *	0.076 ± 0.005	-0.92	8.60	0.128 ± 0.005		52
$Zn-3Mg^{***}$	0.25	-0.902	3.4	0.30		72
Zn-3Mg *** $ECAP-1$	0.18	-0.865	2.7	0.24	SBF	72
Zn-3Mg *** $ECAP-2$	0.19	-0.893	3.2	0.28		72
Zn-1Mg *	-	$\textbf{-}1.09 \pm 0.02$	0.74 ± 0.02	0.012 ± 0.002	DDC	83
Zn-1Mg-0.5Ca *	-	-1.073 ± 0.003	4.3 ± 0.7	0.066 ± 0.004	PBS	83
Zn-1Mg	0.080 ± 0.002	-	-	0.135 ± 0.005	Hamles	55
Zn-1Mg-1Ca	0.092 ± 0.003	-	-	0.170 ± 0.010	Hanks	55
Zn-1.5Mg	0.065 ± 0.015	-	-	0.104 ± 0.040	Hanks	54
Zn-1.5Mg-0.1Ca	0.110 ± 0.015	-	-	0.238 ± 0.045	панкѕ	54
Zn	-	-1.11 ± 0.01	3.02 ± 0.13	0.05 ± 0.01		73
Zn-1Mg-0.1Sr	-	-1.23 ± 0.01	7.85 ± 0.74	0.12 ± 0.01	II1	73
Zn-1Mg-0.1Sr **	-	$\textbf{-}1.19 \pm 0.02$	10.24 ± 3.56	0.15 ± 0.05	Hanks	73
Zn-1Mg-0.5Sr	-	-1.23 ± 0.02	7.13 ± 0.45	0.11 ± 0.01		73
Zn-1Mg-0.1Mn	0.12	-1.23	17.21	0.26	Hanks	56
Zn-1Mg-0.1Mn **	0.11	-1.21	16.76	0.25	папкѕ	56

$ \begin{array}{c ccccccccccccccccccccccccccccccccccc$	56 84 84 84 84 57 55 57 59 59 59
$\begin{array}{cccccccccccccccccccccccccccccccccccc$	84 84 84 84 57 55 57 59 59
$\begin{array}{cccccccccccccccccccccccccccccccccccc$	84 84 84 57 55 57 59 59
$\begin{array}{cccccccccccccccccccccccccccccccccccc$	84 84 57 55 57 59 59
$\begin{array}{cccccccccccccccccccccccccccccccccccc$	84 57 55 57 59 59
$\begin{array}{c ccccccccccccccccccccccccccccccccccc$	57 55 57 59 59 59
$\begin{array}{c ccccccccccccccccccccccccccccccccccc$	55 57 59 59 59
$\begin{array}{c ccccccccccccccccccccccccccccccccccc$	57 59 59 59
$\begin{array}{cccccccccccccccccccccccccccccccccccc$	59 59 59
$\begin{array}{cccccccccccccccccccccccccccccccccccc$	59 59
$ \begin{array}{cccccccccccccccccccccccccccccccccccc$	59
$Zn-3Cu^*$ 0.030 ± 0.004	
Zn-4Cu * 0.025 ± 0.005	59
	3)
7. 20. *	59
Zn-3Cu * 0.012 ± 0.003 -1.102 0.372 0.005	61
Zn-3Cu-0.1Mg * 0.023 ± 0.002 -1.000 1.177 0.018	61
Zn-3Cu-0.5Mg * 0.030 ± 0.003 -0.957 1.563 0.024	61
Zn-3Cu-1Mg * 0.043 ± 0.004 -0.945 12.413 0.180	61
Zn-3Cu * 0.045 ± 0.008 -1.110 ± 0.011 5.8 ± 0.72 0.085	62
Zn-3Cu-0.5Fe * 0.064 ± 0.004 -1.095 ± 0.009 7.1 ± 0.71 0.105 SBF	62
Zn-3Cu-1Fe * 0.069 ± 0.007 -1.087 ± 0.004 8.8 ± 0.35 0.130	62
Zn-0.5Al -0.99 11.08 0.165 ± 0.009	52
Zn-0.5Al * 0.079 ± 0.005 -0.98 9.60 0.143 ± 0.008	52
Zn-1Al -0.99 11.11 0.166 ± 0.007 Hanks	52
Zn-1A1 * 0.078 ± 0.006 -0.98 9.70 0.145 ± 0.007	52
Zn-0.5Al-0.1Mg *** 0.13 ± 0.01 -1.065 ± 0.013 17.3 ± 1.1 -	65
Zn-0.5Al-0.3Mg *** 0.11 ± 0.01 -1.034 ± 0.011 11.2 ± 0.7 - SBF	65
Zn-0.5Al-0.5Mg *** 0.08 ± 0.01 -1.018 ± 0.012 9.5 ± 0.3 -	65
Zn0.85 138 2.71	85
Zn-4Mn1.02 48 0.72 Hanks	85
Zn-24Mn1.35 2.08 0.02	85
Zn * 0.077 ± 0.004 -0.98 ± 0.02 8.9 ± 0.6 0.133 ± 0.010	67
Zn-2.5Ag * 0.079 ± 0.007 -1.12 ± 0.01 9.2 ± 0.9 0.137 ± 0.021	67
Zn-5Ag * 0.081 ± 0.001 -1.12 ± 0.02 9.7 ± 0.7 0.144 ± 0.007	67
Zn-7Ag * 0.084 ± 0.005 -1.14 ± 0.04 9.9 ± 0.6 0.147 ± 0.018	
Zn **1.35 10.96 0.16 SBF	67

Zn-0.2Li **	-	-1.18	3.98	0.06	68
Zn-0.4Li **	-	-1.21	3.80	0.05	68

As cast; * As hot-extruded; ** As hot-rolled; *** As homogenized; ECAP Equal channel angular pressing; SBF: simulated body fluid; PBS: phosphate buffered saline.

In the Zn-Mg alloy system, Dambatta, et al. ⁸⁶ studied the corrosion of as-cast and ECAP-ed Zn-3Mg alloy in SBF (37 °C, pH = 7.4) and found that corrosion was fairly uniform at a rate of 0.21-0.25 mm/year. Alves et al. ⁸⁷ evaluated the corrosion of Zn-1Mg and Zn-2Mg (wt. %) alloys by immersion in SBF up to 6 days and identified the corrosion products as $Zn_5Cl_2(OH)_8$, $Zn_5(CO_3)_2(OH)_6$, $ZnCO_3$, $Zn_3(PO_4)_2$ and $Ca_3Zn_2(PO_4)_2CO_3(OH)_2$. The corrosion rate of pure Zn increased from 0.038 to 0.052 mm/year upon addition of 1 wt.% Mg, however, it decreased to 0.020 mm/year in Zn-2Mg. The initially higher corrosion activity in Zn-1Mg was associated to the presence of Mg⁵² ⁵⁷, whereas the higher Mg contents in Zn-2Mg (wt.%) led to additional stable corrosion products able to provide a more uniform protective layer.

Zou et al. ⁸⁸ studied the corrosion of pure Zn and Zn-xCa alloys (x = 0.5, 1, 2, 3 wt.%) and found that Zn-2Ca corroded the fastest. They attributed this behavior to two-phase boundaries (ZnCa₁₃ and Zn) that create a galvanic coupling. Li, et al. ⁵⁷ also found that Zn-1Ca alloy exhibited a higher corrosion rate than that of Zn-1Mg and pure Zn, but it was still lower than that of Zn-1Sr alloy, which was the fastest corroding sample due to the influence of SrZn₁₃ phase. In ternary Zn-Mg-Sr alloys, Lui et al. ⁷³ observed that the addition of 1 wt.% Mg and 0.1 and 0.5 wt.% Sr doubled the corrosion rate of pure Zn. The small difference of Sr in the alloy did not change the corrosion rate significantly.

Unlike that for Ca, the corrosion rate of Zn decreased with the addition of Mn ⁶⁴. Tested in Hanks' solution, corrosion rates of pure Zn, Zn-4Mn and Zn-24Mn (wt.%) are 2.17, 0.72 and 0.02 mm/year, respectively. Thus, Mn can be used to tailor the corrosion rate of Zn. Liu et al. ⁵⁶ compared the corrosion behavior of as-cast pure-Zn, Zn-1Mg-0.1Mn, Zn-1.5Mg-0.1Mn and as-rolled Zn-1Mg-0.1Mn. After 90 days of immersion, the corrosion rate was ranked in the following order from lowest to highest: pure Zn, as-cast Zn-1Mg-0.1Mn, Zn-1.5Mg-0.1Mn and as-rolled Zn-1Mg-0.1Mn. The effect of 0.5 and 1 wt.% Al on the corrosion behavior of Zn was studied by Mostaed et al. ⁵². It was concluded that Zn-Al alloys exhibited higher corrosion resistance as compared to Zn-Mg alloys, as they present a single phase solid solution microstructure, with no second phase particles leading to galvanic corrosion. Yue et al. ⁶² tested the corrosion of Zn-3Cu,

Zn-3Cu-0.5Fe, Zn-3Cu-1Fe (wt.%) alloys in SBF and found that Fe additions increased the corrosion rate due to the micro-galvanic effect of FeZn₁₃ and CuZn₅ within the Zn matrix.

Sikora-Jasinska et al. 67 investigated the corrosion behavior of Zn-xAg alloys (x = 2.5, 5.0, 7.0 wt. %) in Hanks' solution and found that increased Ag content resulted in an increased of corrosion rate. This trend was associated with the increasing volume fraction of the AgZn₃ phase, which in turn promoted micro-galvanic corrosion between the Ag-rich phase and the Zn. Zhao et al. 68 studied the corrosion response of three binary Zn-xLi alloys (x = 0.2, 0.4 and 0.7 wt%) in SBF for a duration up to 14 days. They found that adding Li in the Zn matrix decreases the corrosion rate due to increasing passivation that was attributed to LiZn₄ phase.

A more representative scenario to investigate the corrosion response of absorbable implants in the human body is obtained through in-vivo corrosion studies in animal models. Bowen, et al. ¹⁰ estimated the in-vivo corrosion rate of Zn implanted in the abdominal aorta of rats from cross-sectional reduction area measurements and found that it increased linearly with additional residence time in the aorta (Figure 4a). In a long-term implantation study, Drelich, et al. ³⁹ demonstrated that Zn wires implanted in the murine artery exhibited a nearly steady corrosion rate for up to at least 20 months post-implantation (Figure 4b), confirming that Zn stents can safely degrade within a time frame from 1 to 2 years. The pure Zn stent conserved its mechanical integrity for 6 months and about half of the stent volume after 12 months (Figure 4c). Yang, et al. ¹¹ reported that the corrosion mechanism of a pure Zn stent in a rabbit abdominal aorta model involved a conversion mechanism in a microenvironment that evolved from the dynamic blood flow to neointima (Figure 4d).

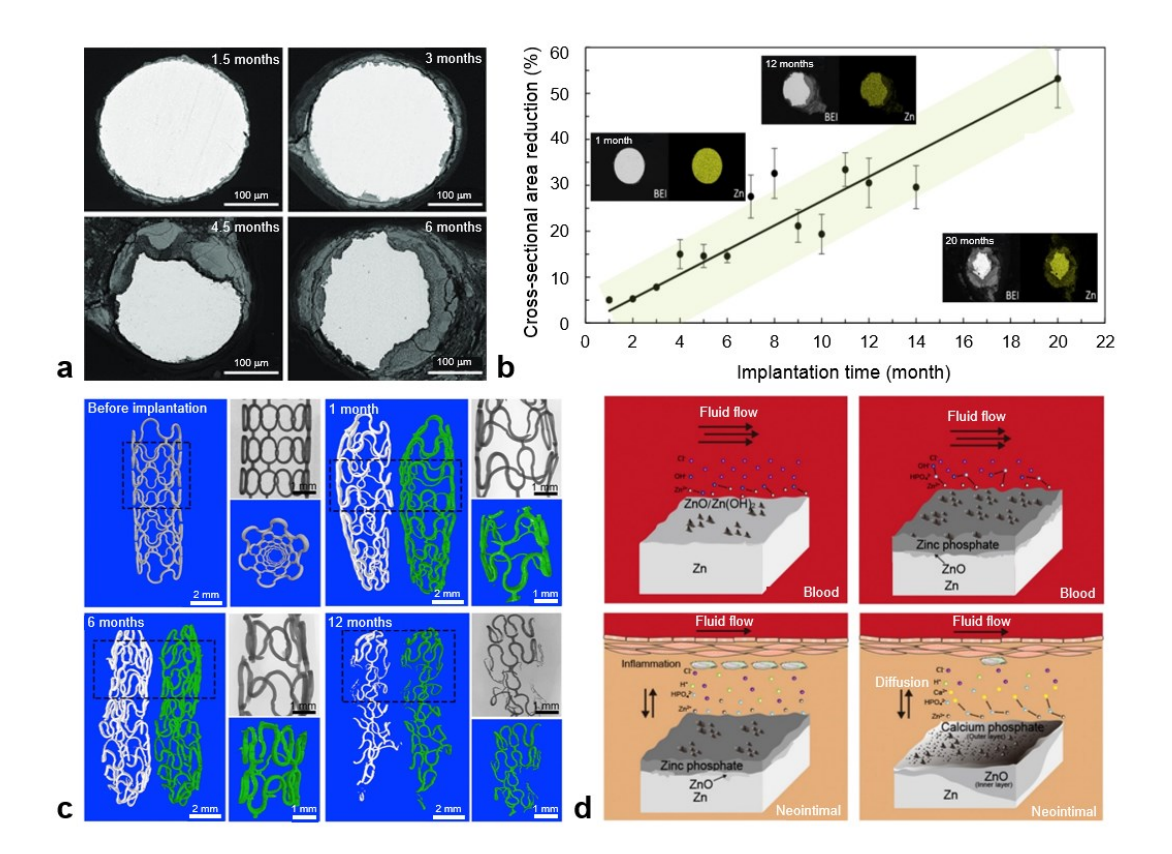


Figure 4: In-vivo corrosion behavior of Zn: (a) cross-sectional changes of Zn explant after 1.5, 3, 4.5 and 6 months in the abdominal aorta of rats, (b) cross-sectional reduction rate of implanted Zn wires as a function of implantation time, (c) micro-CT images of Zn stents after 0, 1, 6 and 12 months of implantation each sowing: a 3D reconstruction among which the white one is the residue Zn stent and the green one represents corrosion products (left); 2D and 3D images of rectangular area of the stent (top right), and a magnified 3D image combining the residue Zn and corrosion products, (d) schematic diagrams showing the evolution of corrosion mechanism of Zn stent from the formation of Zn phosphate under the dynamic flow condition in blood fluid to the conversion of Zn phosphate to ZnO and Ca phosphate under the diffusion condition in the neointimal. Adapted from ^{10,11,39}.

Xiao et al. implanted Zn and Zn-0.05Mg alloy in the femoral shaft of a rabbit for 4, 12 and 24 weeks ³⁶ and observed the presence of Ca around the implant, indicating a bone formation within 12 weeks. Li et al. ⁵⁷ implanted different pins of Zn-1x (x = Mg, Ca, Sr wt.%) alloys in the femora of mice during 0, 1, 2, 3, 4 and 8 weeks (Figure 5a). After only 1 week, the bone surrounding the implantation site of the pins started growing back, showing reactive hyperplasia. It was shown that bone growth occurred significantly faster near the implantation site than in the control group. These studies indicate that alloying with Mg, Ca and Sr can promote new bone formation, which is required for an adequate healing process. The in-vivo corrosion rates were 0.17, 0.19 and 0.22 mm/year for Zn-1Mg, Zn-1Ca and Zn-1Sr (wt. %) respectively.

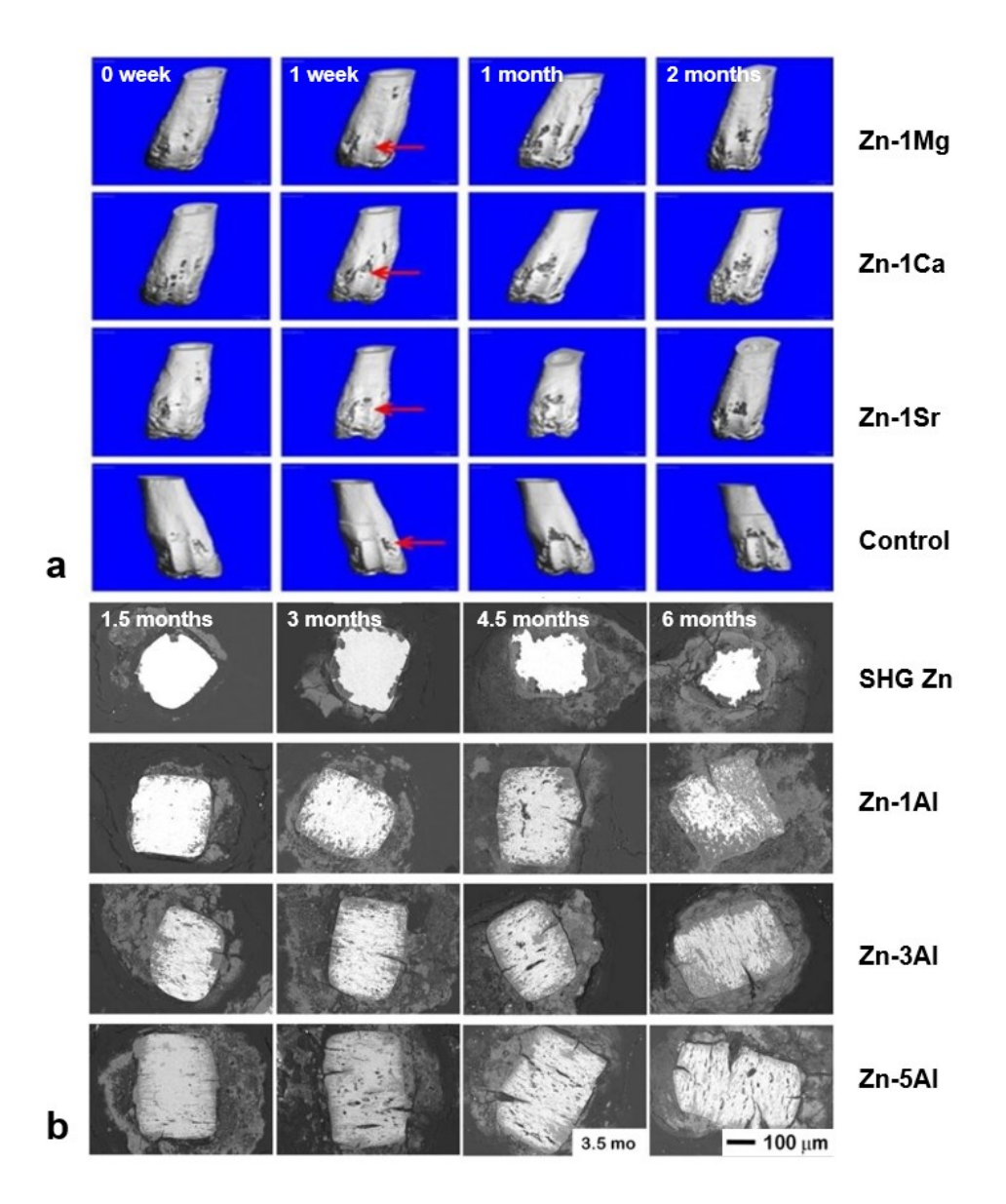


Figure 5: (a) Micro-CT 3D images of Zn-1X pin group and the sham control implanted in the femora of mice, red arrows show the increase in bone density, (b) backscattered electron micrographs of cross sections for SHG Zn, Zn-xAl alloy explants retrieved from rat artery after 1.5, 3, 4.5 (3.5), and 6 months that demonstrate progressions of in-vivo corrosion. Adapted from 51 57

Bowen et al. ⁵¹ implanted strips of special high grade (SHG) Zn and Zn-xAl alloys (x = 1, 3, and 5 wt.%) into the abdominal aorta of adult Sprague-Dawley rats up to 6 months. The corrosion of pure SHG Zn progressed from the implant surface towards the center part, with corrosion products diffusing away from the metal (Figure 5b). It is noted that a portion of the SHG Zn material remains intact after 6 months exposure to the arterial environment, however, the Zn-Al alloys exhibited

earlier degradation and cracking after 1.5 months or sooner. Overall, the in-vivo degradation rate increased with Al content, where the Zn-5Al implant showed the most significant fragmentation among all the Zn-Al alloys studied.

6. Pertinence of Zn-based absorbable alloys for biomedical applications

Despite the fact that pure Zn has exhibited almost ideal corrosion behavior for potential absorbable implants ¹⁰, its mechanical properties are not sufficient for most load-bearing biomedical applications. Consequently, a great number of alloying elements, including, but not limited to Mg, Ca, Sr, Cu, Al, Ag and Li, have been proposed for improving the strength and the ductility of Zn-based alloys while maintaining a desirable corrosion rate and biocompatibility. In most of the investigations related with the development of new alloys, the focus has been on conventional manufacturing processes, such as hot-extrusion and hot-rolling, for which a considerable amount of knowledge gained over the years. Although this has improved the mechanical behavior of Zn-based alloys, i.e. yield and tensile strength and hardness, in general they are not suitable yet to be introduced safely into the market of absorbable medical implants. To help expedite this process, severe plastic deformation (SPD) techniques such as high-pressure torsion (HPT) and equal channel angular pressing (ECAP), are currently being studied and may offer an alternative pathway to achieve a desirable combination of properties.

SPD techniques have demonstrated a substantial potential for ultrafine grain refinement, which has been associated with a balance of high strength and high ductility for a wide range of metals and alloys ^{89–91}. Among these methods, HPT is considered the most promising in terms of producing true bulk nanostructures ⁹². However, the Hall-Petch strengthening associated with grain refinement is limited by a steady-state regime reached at high strain values ⁹³, i.e. 8-10 effective strain ⁹⁴. Thereby, the grain size saturation hinders the improvement of mechanical properties beyond a certain extent when processing is conducted directly on metallic alloys having compositional and microstructural homogeneity. Consequently, alternative methods for synthesizing new metal systems, i.e. Al-Cu, Al-Mg, Al-Fe, Al-Ti, and Zn-Mg, with superior mechanical properties have been obtained by direct diffusion bonding of dissimilar metals through HPT ^{95–98}. Among the metal systems evaluated, the Zn-Mg system exhibits an ultrafine-grained heterogeneous microstructure with presence of HPT-induced intermetallic compounds that contribute to an exceptional hardness ⁹⁹. Moreover, electrochemical studies revealed that the

corrosion resistance and electrochemical kinetics in physiological conditions were similar to that of Zn. This could not only make Zn-Mg hybrids attractive for absorbable biomedical applications, but also guide new researchers in the biomedical field into SPD techniques as an opportunity to achieve the so-called "Paradox of strength and ductility" ¹⁰⁰.

This novel set of metal hybrid systems consist of neighboring domains with different sizes, which create large strain gradients within the material during deformation. This leads to a mechanical incompatibility between soft and hard domains that is accommodated by geometrically necessary dislocations, producing a back-stress work hardening, and thus improving the ε_f. It is precisely this back-stress what provides heterogeneous and/or gradient materials with a superior combination of strength and ductility as compared to their homogeneous counterparts ¹⁰¹. However, besides the mechanical performance, the corrosion properties of the final material must be simultaneously tailored in order to fully satisfy the requirements of the desired implant materials. Each of the phases and/or intermetallic compounds present in the microstructure i.e. Mg₂Zn₁₁, CaZn₁₃, SrZn₁₃, CuZn₅, FeZn₁₃, have their own electrochemical properties, and may act as initiation sites promoting galvanic corrosion upon interaction with the Zn matrix. Therefore, the nature and fraction of the secondary phases, as well as their distribution within the Zn matrix must be investigated carefully, as they will be the primary influencing parameters determining the corrosion behavior in the implant material.

7. Summary and concluding remarks

Bioabsorbable metals should simultaneously fulfill three requirements: have an adequate combination of mechanical properties (i.e. tensile/compressive strength, elongation-to-failure), show acceptable biocompatibility (i.e. not cause toxicity), and posses a corrosion rate matching that of the healing tissue. The first attempts in the development of absorbable metal implants were focused on Fe and Mg-based alloys, which showed promising results, but were generally unable to fully satisfy that demanding set of conditions. As a consequence, Zn was recently introduced in this field due to its outstanding biodegradability and biocompatibility in physiological environment. Moreover, Zn overcomes some of the limitations of Fe and Mg by providing a more suitable range of corrosion rates, similar to those in tissue-healing processes. However, the mechanical strength of Zn is not sufficient for load bearing implantable devices, which has triggered the investigation of biocompatible alloying elements (i.e. Mg, Ca, Sr), and deformation

processes (i.e. rolling, extrusion) towards a search of Zn-based alloys with enhanced mechanical properties. An optimum combination of these two strategies is required to achieve desired microstructural features (i.e. grain size and morphology, size and distribution of second phases and/or intermetallics, crystallographic texture) while maintaining an adequate biocompatibility and corrosion rate.

This review article provides the most current research progress in the development of absorbable Zn-based alloys for biomedical implant applications. The toxicological and metallurgical aspects, as well as the mechanical behavior and corrosion properties of different Zn alloys are presented and discussed, including their opportunities and limitations. In-vitro and in-vivo studies carried out to date have not only shown that Zn-based alloys are not cytotoxic, but also promote osseointegration and tissue healing in the implantation site. Moreover, the mechanical properties after alloying have been greatly improved, and in some case match or exceed the values targeted for either cardiovascular or orthopedic applications. However, due to the low melting point of Zn alloys, several new uncertainties with respect to the mechanical properties may arise, including low creep resistance or high susceptibility to natural aging and static recrystallization, which may lead to medical device failure during storage at RT or implantation at body temperature.

However, it is important to highlight that each biomedical device (i.e. stent, bone plate, screw) requires a unique set of mechanical and corrosion properties, so it is necessary to tailor them accordingly. In addition, the manufacturing techniques (i.e. electrical discharge machining, laser cutting) can also dramatically change the final properties of the implant materials, and thus, it becomes crucial to inspect candidate materials through the processing steps. Similarly, the preliminary results have shown that the corrosion mechanisms and corrosion rates are heavily influenced by the experimental conditions, such as the testing parameters, solution composition, duration of the test or sample surface finish. As a result, it becomes a real challenge to make comprehensive comparisons between different studies reported in the literature. Therefore, there is a need for standards and protocols to deal with this issue while assisting researchers to address the remaining challenges towards the development of Zn-based components to serve the next generation of absorbable biomedical implant applications.

8. Acknowledgments

This work was supported by the Division of Material Research (DMR) of the National Science Foundation (NSF) (Grant No. DMR1607942) through the Metals and Metallic Nanostructures (MMN) program; the Natural Sciences and Engineering Research Council of Canada (NSERC), through the Discovery Grant (Grant No. 638165); and Atatürk University (Grant No. FOA-2018-6525).

9. References

- 1. Hermawan, H. Updates on the research and development of absorbable metals for biomedical applications. *Prog. Biomater.* doi:10.1007/s40204-018-0091-4
- 2. Witte, F. & Eliezer, A. in *Degradation of Implant Materials* (2012). doi:10.1007/978-1-4614-3942-4_5
- 3. Pietrzak, W. S. & Eppley, B. L. Resorbable polymer fixation for craniomaxillofacial surgery: development and engineering paradigms. *J. Craniofac. Surg.* **11**, 575–85 (2000).
- 4. Francis, A., Yang, Y., Virtanen, S. & Boccaccini, A. R. Iron and iron-based alloys for temporary cardiovascular applications. *J. Mater. Sci. Mater. Med.* **26**, 138 (2015).
- 5. Bosiers, M. *et al.* AMS INSIGHT--absorbable metal stent implantation for treatment of below-the-knee critical limb ischemia: 6-month analysis. *Cardiovasc. Intervent. Radiol.* **32**, 424–35 (2009).
- 6. Windhagen, H. *et al.* Biodegradable magnesium-based screw clinically equivalent to titanium screw in hallux valgus surgery: short term results of the first prospective, randomized, controlled clinical pilot study. *Biomed. Eng. Online* **12**, 62 (2013).
- 7. Gu, X., Zheng, Y., Cheng, Y., Zhong, S. & Xi, T. In vitro corrosion and biocompatibility of binary magnesium alloys. *Biomaterials* **30**, 484–498 (2009).
- 8. Pierson, D. *et al.* A simplified in vivo approach for evaluating the bioabsorbable behavior of candidate stent materials. *J. Biomed. Mater. Res. Part B Appl. Biomater.* **100B**, 58–67 (2012).
- 9. Vojtěch, D., Kubásek, J., Šerák, J. & Novák, P. Mechanical and corrosion properties of newly developed biodegradable Zn-based alloys for bone fixation. *Acta Biomater*. (2011). doi:10.1016/j.actbio.2011.05.008
- 10. Bowen, P. K., Drelich, J. & Goldman, J. Zinc exhibits ideal physiological corrosion behavior for bioabsorbable stents. *Adv. Mater.* (2013). doi:10.1002/adma.201300226
- 11. Yang, H. *et al.* Evolution of the degradation mechanism of pure zinc stent in the one-year study of rabbit abdominal aorta model. *Biomaterials* **145**, 92–105 (2017).
- 12. McCall, K. A., Huang, C. & Fierke, C. A. Function and Mechanism of Zinc

- Metalloenzymes. J. Nutr. 130, 1437S–1446S (2000).
- 13. Brown, K. H., Peerson, J. M., Rivera, J. & Allen, L. H. Effect of supplemental zinc on the growth and serum zinc concentrations of prepubertal children: a meta-analysis of randomized controlled trials. *Am. J. Clin. Nutr.* **75**, 1062–1071 (2002).
- 14. International Zinc Nutrition Consultative Group (IZiNCG) *et al.* International Zinc Nutrition Consultative Group (IZiNCG) technical document #1. Assessment of the risk of zinc deficiency in populations and options for its control. *Food Nutr. Bull.* **25**, S99-203 (2004).
- 15. Fosmire, G. J. Zinc toxicity. *Am. J. Clin. Nutr.* **51**, 225–227 (1990).
- 16. Fairweather-Tait, S. & Hurrell, R. F. Bioavailability of Minerals and Trace Elements. *Nutr. Res. Rev.* **9**, 295 (1996).
- 17. Cousins, R. J. Absorption, transport, and hepatic metabolism of copper and zinc: special reference to metallothionein and ceruloplasmin. *Physiol. Rev.* **65**, 238–309 (1985).
- 18. Nriagu, J. Zinc Toxicity in Humans Introduction Functions of Zinc in Humans Epidemiology Acute Health Effects Chronic and Subchronic Toxicity Potential for Zinc Accumulation Further Reading.
- 19. Krebs, N. F. Overview of Zinc Absorption and Excretion in the Human Gastrointestinal Tract. *J. Nutr.* **130**, 1374S–1377S (2000).
- Kambe, T., Tsuji, T., Hashimoto, A. & Itsumura, N. The Physiological, Biochemical, and Molecular Roles of Zinc Transporters in Zinc Homeostasis and Metabolism. *Physiol. Rev.* 95, 749–784 (2015).
- 21. Plum, L. M., Rink, L. & Haase, H. The Essential Toxin: Impact of Zinc on Human Health. *Int. J. Environ. Res. Public Health* 7, 1342–1365 (2010).
- 22. Bartzatt, R. Neurological Impact of Zinc Excess and Deficiency In vivo. *Eur. J. Nutr. Food Saf.* **7,** (2017).
- 23. Little, P. J., Bhattacharya, R., Moreyra, A. E. & Korichneva, I. L. Zinc and cardiovascular disease. *Nutrition* **26**, 1050–7 (2010).
- 24. Mohammad, M. K., Zhou, Z., Cave, M., Barve, A. & McClain, C. J. Zinc and Liver Disease.

- Nutr. Clin. Pract. 27, 8–20 (2012).
- 25. Lobo, J. C., Torres, J. P. M., Fouque, D. & Mafra, D. Zinc deficiency in Chronic Kidney Disease: Is there a Relationship with Adipose Tissue and Atherosclerosis? *Biol. Trace Elem. Res.* **135**, 16–21 (2010).
- 26. Roohani, N., Hurrell, R., Kelishadi, R. & Schulin, R. Zinc and its importance for human health: An integrative review. *J. Res. Med. Sci.* **18,** 144–57 (2013).
- 27. Shankar, A. H. & Prasad, A. S. Zinc and immune function: the biological basis of altered resistance to infection. *Am. J. Clin. Nutr.* **68,** 447S–463S (1998).
- 28. Dardenne, M. Zinc and immune function. Eur. J. Clin. Nutr. 56, 20–23 (2002).
- 29. Hickory, W., Nanda, R. & Catalanotto, F. A. Fetal Skeletal Malformations Associated with Moderate Zinc Deficiency During Pregnancy.
- 30. Hambidge, M. & Krebs, N. F. INTERRELATIONSHIPS OF KEY VARIABLES OF HUMAN ZINC HOMEOSTASIS: Relevance to Dietary Zinc Requirements. *Annu. Rev. Nutr.* **21**, 429–452 (2001).
- 31. Johnson, P. E., Hunt, C. D., Milne, D. B. & Mullen, L. K. Homeostatic control of zinc metabolism in men: zinc excretion and balance in men fed diets low in zinc. *Am. J. Clin. Nutr.* **57**, 557–565 (1993).
- 32. Maret, W. & Sandstead, H. H. Zinc requirements and the risks and benefits of zinc supplementation. *J. Trace Elem. Med. Biol.* **20**, 3–18 (2006).
- 33. Murni, N. S., Dambatta, M. S., Yeap, S. K., Froemming, G. R. A. & Hermawan, H. Cytotoxicity evaluation of biodegradable Zn-3Mg alloy toward normal human osteoblast cells. *Mater. Sci. Eng. C* (2015). doi:10.1016/j.msec.2015.01.056
- 34. Shearier, E. R. *et al.* In Vitro Cytotoxicity, Adhesion, and Proliferation of Human Vascular Cells Exposed to Zinc. *ACS Biomater. Sci. Eng.* **2,** 634–642 (2016).
- 35. Ma, J., Zhao, N. & Zhu, D. Bioabsorbable zinc ion induced biphasic cellular responses in vascular smooth muscle cells. *Sci. Rep.* **6**, 26661 (2016).
- 36. Xiao, C. *et al.* Indirectly extruded biodegradable Zn-0.05wt%Mg alloy with improved strength and ductility: In vitro and in vivo studies. *J. Mater. Sci. Technol.* (2018).

- doi:10.1016/J.JMST.2018.01.006
- 37. Bowen, P. K. *et al.* Metallic zinc exhibits optimal biocompatibility for bioabsorbable endovascular stents. *Mater. Sci. Eng. C* (2015). doi:10.1016/j.msec.2015.07.022
- 38. Guillory, R. J. *et al.* Corrosion Characteristics Dictate the Long-Term Inflammatory Profile of Degradable Zinc Arterial Implants. *ACS Biomater. Sci. Eng.* **2**, 2355–2364 (2016).
- 39. Drelich, A. J., Zhao, S., Guillory, R. J., Drelich, J. W. & Goldman, J. Long-term surveillance of zinc implant in murine artery: Surprisingly steady biocorrosion rate. *Acta Biomater.* **58**, 539–549 (2017).
- 40. Van Nostrand's Encyclopedia of Chemistry. 1–14 (2005).
- 41. International Lead and Zinc Study Group Statistics. Available at: http://www.ilzsg.org/static/statistics.aspx?from=1.
- 42. Hot-Dip Galvanizing Vs. Zinc Electroplating Pipeline & Samp; Gas Journal. Available at: https://pgjonline.com/2013/03/27/hot-dip-galvanizing-vs-zinc-electroplating/.
- 43. Zinc processing Encyclopedia Britannica. Available at: https://www.britannica.com/technology/zinc-processing.
- 44. Composition of Common Brass Alloys. Available at: https://www.thebalance.com/composition-of-common-brass-alloys-2340109.
- 45. North American Die Casting Association NADCA design. Available at: http://www.diecastingdesign.org/zinc-alloys.
- 46. ASM Handbook: Vol. 2. Zinc and Zinc Alloys (1992).
- 47. Linch, R. F. (Lynch & A. I. Zinc: Alloying, Thermomechanical Processing, Properties, and Applications. 5000–5000
- 48. Hercz, G. *et al.* Reversal of Aluminum-Related Bone Disease After Substituting Calcium Carbonate for Aluminum Hydroxide. *Am. J. Kidney Dis.* **11,** 70–75 (1988).
- 49. Dunea, G., Mahurkar, S. D., Mamdani, B. & Smith, E. C. Role of aluminum in dialysis dementia. *Ann. Intern. Med.* **88**, 502–4 (1978).
- 50. Mirza, A., King, A., Troakes, C. & Exley, C. Aluminium in brain tissue in familial

- Alzheimer's disease. J. Trace Elem. Med. Biol. 40, 30–36 (2017).
- 51. Bowen, P. K. *et al.* Evaluation of wrought Zn-Al alloys (1, 3, and 5 wt % Al) through mechanical and in vivo testing for stent applications. *J. Biomed. Mater. Res. Part B Appl. Biomater.* 245–258 (2017). doi:10.1002/jbm.b.33850
- 52. Mostaed, E. *et al.* Novel Zn-based alloys for biodegradable stent applications: Design, development and in vitro degradation. *J. Mech. Behav. Biomed. Mater.* (2016). doi:10.1016/j.jmbbm.2016.03.018
- 53. Jin, H. *et al.* Novel high-strength, low-alloys Zn-Mg (< 0.1 wt% Mg) and their arterial biodegradation. *Mater. Sci. Eng. C* **84,** 67–79 (2017).
- 54. Liu, X. *et al.* Effects of alloying elements (Ca and Sr) on microstructure, mechanical property and in vitro corrosion behavior of biodegradable Zn-1.5Mg alloy. *J. Alloys Compd.* **664**, 444–452 (2016).
- 55. Li, H. *et al.* Design and characterizations of novel biodegradable ternary Zn-based alloys with IIA nutrient alloying elements Mg, Ca and Sr. *Mater. Des.* **83**, 95–102 (2015).
- 56. Liu, X. et al. Micro-alloying with Mn in Zn-Mg alloy for future biodegradable metals application. *Mater. Des.* **94,** 95–104 (2016).
- 57. Li, H. F. *et al.* Development of biodegradable Zn-1X binary alloys with nutrient alloying elements Mg, Ca and Sr. *Sci. Rep.* **5**, 1–14 (2015).
- 58. Brandes, E. A. & Brook, G. B. *Smithells Metals Reference Book*. (Oxford: Butterworth-Heinemann, 1992). doi:10.1016/B978-075067509-3/50014-2
- 59. Tang, Z. *et al.* Potential biodegradable Zn-Cu binary alloys developed for cardiovascular implant applications. *J. Mech. Behav. Biomed. Mater.* **72,** 182–191 (2017).
- 60. Niu, J. *et al.* Research on a Zn-Cu alloy as a biodegradable material for potential vascular stents application. *Mater. Sci. Eng. C* **69**, 407–413 (2016).
- 61. Tang, Z. *et al.* Design and characterizations of novel biodegradable Zn-Cu-Mg alloys for potential biodegradable implants. *Mater. Des.* **117**, 84–94 (2017).
- 62. Yue, R. *et al.* Microstructure, mechanical properties and in vitro degradation behavior of novel Zn-Cu-Fe alloys. *Mater. Charact.* **134,** 114–122 (2017).

- 63. Sun, S. *et al.* Abnormal effect of Mn addition on the mechanical properties of as-extruded Zn alloys. *Mater. Sci. Eng. A* **701**, 129–133 (2017).
- 64. Sotoudeh Bagha, P., Khaleghpanah, S., Sheibani, S., Khakbiz, M. & Zakeri, A. Characterization of nanostructured biodegradable Zn-Mn alloy synthesized by mechanical alloying. *J. Alloys Compd.* **735**, 1319–1327 (2018).
- 65. Bakhsheshi-Rad, H. R. *et al.* Fabrication of biodegradable Zn-Al-Mg alloy: Mechanical properties, corrosion behavior, cytotoxicity and antibacterial activities. *Mater. Sci. Eng. C* 73, 215–219 (2017).
- 66. Bakhsheshi-Rad, H. R. *et al.* Thermal characteristics, mechanical properties, in vitro degradation and cytotoxicity of novel biodegradable Zn-Al-Mg and Zn-Al-Mg-xBi alloys. *Acta Metall. Sin. (English Lett.* **30**, 201–211 (2017).
- 67. Sikora-Jasinska, M. *et al.* Fabrication, mechanical properties and in vitro degradation behavior of newly developed Zn-Ag alloys for degradable implant applications. *Mater. Sci. Eng. C* 77, 1170–1181 (2017).
- 68. Zhao, S. *et al.* Structural Characteristics and In Vitro Biodegradation of a Novel Zn-Li Alloy Prepared by Induction Melting and Hot Rolling. *Metall. Mater. Trans. A Phys. Metall. Mater. Sci.* **48**, 1204–1215 (2017).
- 69. ASTM B86-18: Standard Specification for Zinc and Zinc-Aluminum (ZA) Alloy Foundry and Die Castings (2019). doi:10.1520/B0086-18
- 70. Jarzębska, A. *et al.* A new approach to plastic deformation of biodegradable zinc alloy with magnesium and its effect on microstructure and mechanical properties. *Mater. Lett.* **211,** 58–61 (2018).
- 71. Shen, C. *et al.* Mechanical properties, in vitro degradation behavior, hemocompatibility and cytotoxicity evaluation of Zn–1.2Mg alloy for biodegradable implants. *RSC Adv.* **6**, 86410–86419 (2016).
- 72. Dambatta, M. S., Izman, S., Kurniawan, D. & Hermawan, H. Processing of Zn-3Mg alloy by equal channel angular pressing for biodegradable metal implants. *J. King Saud Univ. Sci.* **29**, 455–461 (2017).

- 73. Liu, X. *et al.* Microstructure, mechanical properties, in vitro degradation behavior and hemocompatibility of novel Zn–Mg–Sr alloys as biodegradable metals. *Mater. Lett.* **162**, 242–245 (2016).
- 74. MatWeb Material Property Data. Available at: http://www.matweb.com/.
- 75. Li, H., Zheng, Y. & Qin, L. Progress of biodegradable metals. *Prog. Nat. Sci. Mater. Int.* **24,** 414–422 (2014).
- 76. de la Fuente, D., Castaño, J. G. & Morcillo, M. Long-term atmospheric corrosion of zinc. *Corros. Sci.* **49**, 1420–1436 (2007).
- 77. Tafreshi, M., Allahkaram, S. R. & Farhangi, H. Comparative study on structure, corrosion properties and tribological behavior of pure Zn and different Zn-Ni alloy coatings. *Mater. Chem. Phys.* **183**, 263–272 (2016).
- 78. Standard Test Method for Conducting Cyclic Potentiodynamic Polarization Measurements to Determine the Corrosion Susceptibility of Small Implant Devices. doi:10.1520/F2129-17B
- 79. Törne, K., Larsson, M., Norlin, A. & Weissenrieder, J. Degradation of zinc in saline solutions, plasma, and whole blood. *J. Biomed. Mater. Res. Part B Appl. Biomater.* **104,** 1141–1151 (2016).
- 80. Chen, Y. *et al.* Comparative corrosion behavior of Zn with Fe and Mg in the course of immersion degradation in phosphate buffered saline. *Corros. Sci.* **111**, 541–555 (2016).
- 81. Krężel, A. & Maret, W. The biological inorganic chemistry of zinc ions. *Arch. Biochem. Biophys.* **611**, 3–19 (2016).
- 82. Thomas, S., Birbilis, N., Venkatraman, M. S. & Cole, I. S. Corrosion of Zinc as a Function of pH. *CORROSION* **68**, 015009-1-015009-9 (2012).
- 83. Katarivas Levy, G. *et al.* Evaluation of biodegradable Zn-1%Mg and Zn-1%Mg-0.5%Ca alloys for biomedical applications. *J. Mater. Sci. Mater. Med.* **28,** 174 (2017).
- 84. Zou, Y., Chen, X. & Chen, B. Effects of Ca concentration on degradation behavior of Zn-x Ca alloys in Hank's solution. *Mater. Lett.* **218**, 193–196 (2018).
- 85. Sotoudeh Bagha, P., Khaleghpanah, S., Sheibani, S., Khakbiz, M. & Zakeri, A.

- Characterization of nanostructured biodegradable Zn-Mn alloy synthesized by mechanical alloying. *J. Alloys Compd.* **735,** 1319–1327 (2018).
- 86. Dambatta, M. S. *et al.* Influence of thermal treatment on microstructure, mechanical and degradation properties of Zn-3Mg alloy as potential biodegradable implant material. *Mater. Des.* (2015). doi:10.1016/j.matdes.2015.06.181
- 87. Alves, M. M., Prošek, T., Santos, C. F. & Montemor, M. F. Evolution of the in vitro degradation of Zn–Mg alloys under simulated physiological conditions. *RSC Adv.* 7, 28224–28233 (2017).
- 88. Zou, Y., Chen, X. & Chen, B. Effects of Ca concentration on degradation behavior of Zn-x Ca alloys in Hank's solution. *Mater. Lett.* **218**, 193–196 (2018).
- 89. Ma, E. & Zhu, T. Towards strength–ductility synergy through the design of heterogeneous nanostructures in metals. *Mater. Today* **20,** 323–331 (2017).
- 90. Wang, Y., Chen, M., Zhou, F. & Ma, E. High tensile ductility in a nanostructured metal. *Nature* **419**, 912–915 (2002).
- 91. Wang, L., Shi, Y., Zhang, Y. & Li, M. High tensile ductility and strength in a gradient structured Zr. *Mater. Lett.* **228**, 500–503 (2018).
- 92. Zhilyaev, A. P. & Langdon, T. G. Using high-pressure torsion for metal processing: Fundamentals and applications. *Prog. Mater. Sci.* **53**, 893–979 (2008).
- 93. Edalati, K., Miresmaeili, R., Horita, Z., Kanayama, H. & Pippan, R. Significance of temperature increase in processing by high-pressure torsion. *Mater. Sci. Eng. A* **528**, 7301–7305 (2011).
- 94. Kapoor, R. in *Materials Under Extreme Conditions* 717–754 (Elsevier, 2017). doi:10.1016/B978-0-12-801300-7.00020-6
- 95. Oh-ishi, K., Edalati, K., Kim, H. S., Hono, K. & Horita, Z. High-pressure torsion for enhanced atomic diffusion and promoting solid-state reactions in the aluminum-copper system. *Acta Mater.* **61**, 3482–3489 (2013).
- 96. Kawasaki, M., Ahn, B., Lee, H.-J., Zhilyaev, A. P. & Langdon, T. G. Using high-pressure torsion to process an aluminum-magnesium nanocomposite through diffusion bonding. *Acta*

- *Mater.* **59,** 1974–1985 (2015).
- 97. Ahn, B., Zhilyaev, A. P., Lee, H. J., Kawasaki, M. & Langdon, T. G. Rapid synthesis of an extra hard metal matrix nanocomposite at ambient temperature. *Mater. Sci. Eng. A* **635**, 109–117 (2015).
- 98. Kawasaki, M., Han, J.-K., Lee, D.-H., Jang, J. & Langdon, T. G. Fabrication of nanocomposites through diffusion bonding under high-pressure torsion. *J. Mater. Res.* 1–11 (2018). doi:10.1557/jmr.2018.205
- 99. Hernández-Escobar, D., Rahman, Z. U., Yilmazer, H., Kawasaki, M. & Boehlert, C. J. Microstructural evolution and intermetallic formation in Zn-Mg hybrids processed by High-Pressure Torsion. *Philos. Mag.* 1–28 (2018). doi:10.1080/14786435.2018.1546962
- 100. Valiev, R. Z., Alexandrov, I. V, Zhu, Y. T. & Lowe, T. C. Paradox of strength and ductility in metals processed by severe plastic deformation. *J. Mater. Res.* **17,** 5–8 (2002).
- 101. Wu, X. & Zhu, Y. Heterogeneous materials: a new class of materials with unprecedented mechanical properties. **5**, 527–532 (2017).